Catalysis Communications 34 (2013) 58–63

Contents lists available at SciVerse ScienceDirect

Catalysis Communications

journal homepage: www.elsevier.com/locate/catcom

Short Communication

One-step synthesis of mesoporous $H_4SiW_{12}O_{40}$-SiO_2 catalysts for the production of methyl and ethyl levulinate biodiesel

Kai Yan, Guosheng Wu, Jiali Wen, Aicheng Chen *

Department of Chemistry, Lakehead University, 955 Oliver Road, Thunder Bay, ON, Canada P7B 5E1

A R T I C L E   I N F O

Article history:
Received 19 November 2012
Received in revised form 6 January 2013
Accepted 8 January 2013
Available online 20 January 2013

Keywords:
One-step synthesis
Mesoporous materials
$H_4SiW_{12}O_{40}$-SiO_2
Catalysis
Biodiesel

A B S T R A C T

A novel one-step method for the synthesis of mesoporous $H_4SiW_{12}O_{40}$-SiO_2 catalysts with tunable composition was successfully developed using non-ionic polyethylene glycol dodecyl ether (Brij 30) as the structure-directing template. Different loadings of $H_4SiW_{12}O_{40}$ (up to 30 wt.%) were effectively confined within the mesoporous channels of SiO_2, which would facilitate easy recycling and allow for the efficient mass transport of reactants and products. The resultant mesoporous $H_4SiW_{12}O_{40}$-SiO_2 showed high catalytic activity for the production of methyl and ethyl levulinate biodiesel. The 20 wt.% $H_4SiW_{12}O_{40}$-SiO_2 catalyst exhibited the best performance in the synthesis of both methyl levulinate (73% yield achieved at 79% conversion of levulinic acid) and ethyl levulinate (67% yield obtained at 75% conversion of levulinic acid).

1. Introduction

With the inevitable depletion of non-renewable petroleum resources and growing environmental concerns associated with their use, renewable biomass is increasingly regarded as a promising alternative for the sustainable supply of fuels and chemicals [1,2]. Substantial research efforts have been invested in the conversion of biomass or biomass-derived chemicals to biofuels and value-added chemicals [3–5]. Among these investigations, it has been elucidated that methyl levulinate (ML) and ethyl levulinate (EL) are very attractive candidates as novel miscible diesel biofuels [6,7]. These biofuels may be synthesized from levulinic acid and alkyl alcohol, where the levulinic acid is produced from renewable lignocellulosic biomass [1,8]. Due to their unique properties, ML and EL are suitable for use as additives for gasoline and diesel transportation fuels, which have manifold excellent performance attributes, such as non-toxicity, high lubricity, flashpoint stability and superior flow properties under cold conditions [9–12].

Traditionally utilized catalysts for the production of esters often focused on homogeneous mineral acids such as formic acid, H_3PO_4 and H_2SO_4 [13–15]. Although high yields have been achieved, the handling of mineral acids as well as corrosion and recycling issues have been problematic. Due to their ease of recycling and separation, heterogeneous catalysts have gained appeal. Zeolite and heteropoly acid are the most often employed catalysts for esterification due to benefits such as adjustable acidity, simple recyclability, economic potential and environmental compatibility [16–18]. Recently, Riisager et al. studied sulfonic acid functionalized SBA-15, sulfated zirconia and beta, Y, ZSM-5 and mordenite zeolite catalysts for the conversion of fructose to EL utilizing ethanol as the solvent and reactant. A 57% yield of EL was obtained on sulphonic acid functionalized SBA-15 at 140 °C [19]. More recently, Baronetti et al. reported a Wells–Dawson heteropoly acid that was supported on silicon gel for the synthesis of EL from levulinic acid and ethanol [20]. A 76% yield was achieved, where the weak heteropoly acid is the catalytic active center [21,22].

There are great interests in the development of new and environmentally benign technologies for the efficient synthesis of ML and EL. Mesoporous SiO_2 with suitable pore sizes has the capacity to confine the catalytic active species heteropoly acid, which facilitates easy recycling, and allows for the efficient mass transport of reactants and products. In this study, we have developed a novel one-step method for the synthesis of $H_4SiW_{12}O_{40}$-SiO_2 catalyst using a new heteropoly acid (Keggin Unit, $H_4SiW_{12}O_{40}$) that is confined within the mesoporous channels of SiO_2. The surfactant Brij30 was utilized for the first time as a structure directing agent in the formation of mesoporous $H_4SiW_{12}O_{40}$-SiO_2. The resultant mesoporous $H_4SiW_{12}O_{40}$-SiO_2 catalysts were shown to be highly efficient for the production of ML and EL biodiesel.

2. Experimental

2.1. Synthesis and characterization of mesoporous $H_4SiW_{12}O_{40}$-SiO_2

Details on the reagents that were used in this study are described in the supplementary information. The one-step synthesis was facilitated in the presence of the surfactant Brij30. Firstly, 1.3 g Brij30 was dissolved in a 25 mL HCl solution for 12 h under 40 °C. Secondly, a mixture of

---

* Corresponding author. Tel.: +1 807 3438318.
E-mail address: aicheng.chen@lakeheadu.ca (A. Chen).

1566-7367/$ – see front matter © 2013 Elsevier B.V. All rights reserved.
http://dx.doi.org/10.1016/j.catcom.2013.01.010

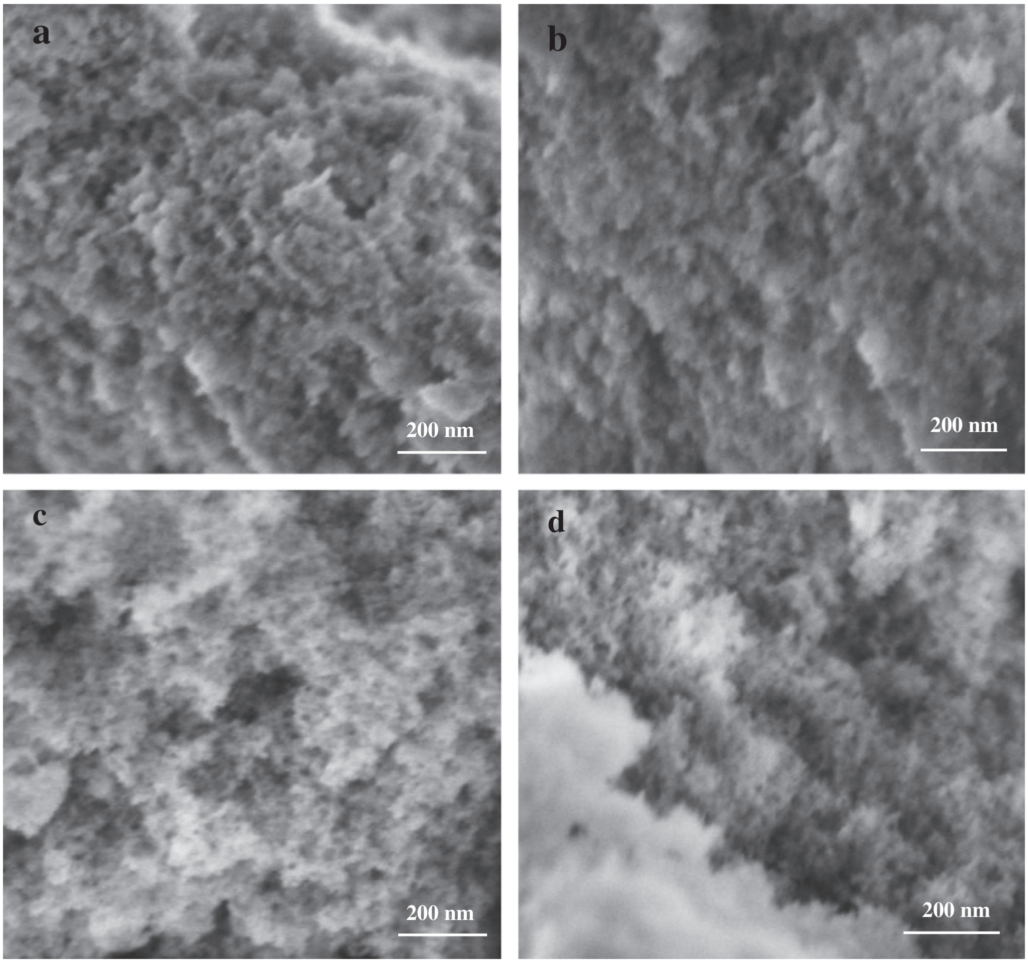

Fig. 1. SEM analysis of different $H_4SiW_{12}O_{40}$ loadings inside SiO_2: (a) mesoporous SiO_2; (b) 10 wt.% $H_4SiW_{12}O_{40}$-SiO_2; (c) 20 wt.% $H_4SiW_{12}O_{40}$-SiO_2; (d) 30 wt.% $H_4SiW_{12}O_{40}$-SiO_2.

2.4 mL tetraethyl orthosilicate and 2.0 mL ethanol was added. Subsequently, a pre-determined amount of Keggin Unit tungstosilicic acid hydrate ($H_4SiW_{12}O_{40}$), for instance 0.065 g for 10 wt.% loading, was added to the Brij30/HCl solution. The resulting suspension was blended at 40 °C for 24 h, and then heated at 100 °C for 24 h. Finally, the obtained gel was rinsed with pure water, dried at 90 °C overnight and calcinated at 350 °C for 8 h. The 10 wt.% tungstosilicic acid hydrate loading was designated as 10 wt.% $H_4SiW_{12}O_{40}$-SiO_2. For comparison, mesoporous SiO_2 was also prepared using the same procedure in the absence of tungstosilicic acid hydrate. The synthesized mesoporous SiO_2 and $H_4SiW_{12}O_{40}$-SiO_2 catalysts were characterized by X-ray diffraction (XRD), N_2 adsorption/desorption (N_2-BET), transmission electron microscopy (TEM), scanning electron microscopy (SEM), Fourier transform infrared spectroscopy (FT-IR), energy dispersive X-ray analysis (EDX) and inductively coupled plasma-mass spectroscopy (ICP-MS). Details are presented in the Supplementary information.

2.2. Catalytic synthesis of levulinate esters

The synthesis of ML and EL was performed in a flask that was coupled with a thermometer and reflux condenser. In a typical run, levulinic acid (205 mg) was dissolved in 2 mL methanol or ethanol, followed by the addition of the $H_4SiW_{12}O_{40}$-SiO_2 catalyst (104 mg) and cyclohexane (5 mL) as the solvent. The flask was heated for 6 h at an agitation speed of 1000 rpm, where the temperature was maintained at 65 and 75 °C for the synthesis of ML and EL, respectively. Following the reaction, the reactants and products were analyzed by gas chromatography (Shimadzu GC 2014; column: 30 m DBWaxetr, FID) and high performance liquid chromatography (Shimadzu LC10; column: organic acid resin; UV detector).

3. Results and discussion

3.1. Catalyst characterization

The XRD patterns of pure $H_4SiW_{12}O_{40}$, the synthesized SiO_2 and $H_4SiW_{12}O_{40}$-SiO_2 catalysts are presented in the Supplementary information (Fig. S1). A broad diffraction peak that ranged from 20 to 30°, which can be attributed to the amorphous silica [23–26], was observed when the $H_4SiW_{12}O_{40}$ loadings were lower than 30 wt.% (Fig. S1, b to e). However, the diffraction peaks corresponding to $H_4SiW_{12}O_{40}$ were imperceptible, indicating that the loaded $H_4SiW_{12}O_{40}$ was effectively confined within the mesoporous channels of the SiO_2. When the $H_4SiW_{12}O_{40}$ loading was increased to 40 wt.% (Fig. S1f), two small peaks appeared at 8.3° and 25.8°. Meanwhile, the silica peak centered at ~24° became broader and weaker, signifying that high $H_4SiW_{12}O_{40}$ loading (40 wt.%) might deform the silica skeleton and thus partially disorder the mesoporous channels of SiO_2. In addition, high $H_4SiW_{12}O_{40}$ loading might result in uneven dispersion or aggregation [23].

FT-IR analysis was further employed to identify the structural evolution of the catalyst. The FTIR spectra of the mesoporous SiO_2 and 20 wt.% $H_4SiW_{12}O_{40}$-SiO_2 samples are shown in Fig. S2. The characteristic bands of the mesoporous SiO_2 (Fig. S2a) appeared at 820 (Si – O bending) and 1063 cm^{-1} (Si – O – Si stretching). Subsequent to the introduction of 20 wt.% $H_4SiW_{12}O_{40}$ in the mesoporous SiO_2, the catalyst displayed characteristic bonds at 970 cm^{-1} (W═O, terminal bonds), 920 and

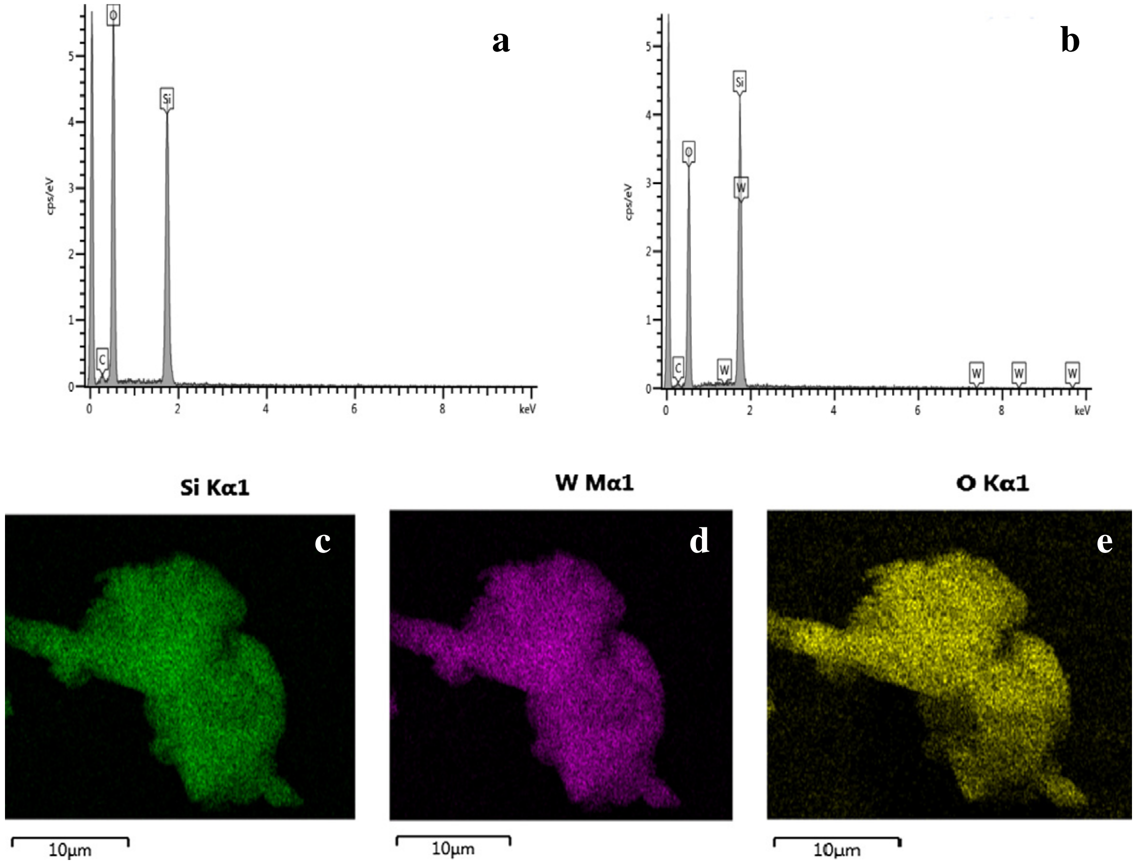

Fig. 2. EDX analysis spectrum and EDX mapping of 20 wt.% $H_4SiW_{12}O_{40}$-SiO_2 : (a) mesoporous SiO_2; (b) 10 wt.% $H_4SiW_{12}O_{40}$-SiO_2; (c) silica in 20 wt.% $H_4SiW_{12}O_{40}$-SiO_2; (d) tungsten in 20 wt.% $H_4SiW_{12}O_{40}$-SiO_2; (e) oxygen in 20 wt.% $H_4SiW_{12}O_{40}$-SiO_2.

790 cm^{-1} (W–O–W bridges), respectively. This indicates that the $H_4SiW_{12}O_{40}$ maintained its Keggin Unit following the synthesis [20,27].

SEM and EDX were further employed to elucidate further morphological and compositional data of the synthesized catalysts. As shown in Fig. 1, the representative SEM images of the mesoporous SiO_2 (*a*), 10 wt.% $H_4SiW_{12}O_{40}$-SiO_2 (*b*) and 20 wt.% $H_4SiW_{12}O_{40}$-SiO_2 (*c*) displayed similar morphologies with an interconnected pore/network structure. However, when the $H_4SiW_{12}O_{40}$ loading was 30 wt.% (Fig. 1d), some aggregation was formed on the surface, which is consistent with the aforementioned XRD results. Fig. 2a and b presents the EDX spectra of the mesoporous SiO_2 and 10 wt.% $H_4SiW_{12}O_{40}$-SiO_2, respectively. Strong oxygen and silicon peaks were observed and a number of tungsten peaks appeared in Fig. 2b, evidencing the existence of tungsten in the sample. However, the strongest tungsten peak was partially overlapped with the silica peak. EDX mapping was further utilized to verify the homogeneous element distribution. A high degree dispersion of the Si, W and O elements was found in the 20 wt.% $H_4SiW_{12}O_{40}$-SiO_2 sample (Fig. 2c–e).

Fig. 3 displays the representative TEM images of 20 wt.% $H_4SiW_{12}O_{40}$-SiO_2. As seen from Fig. 3a, the synthesized catalyst exhibited the interconnected porous-network structure with high porosity and no notable aggregation was detected. The high-

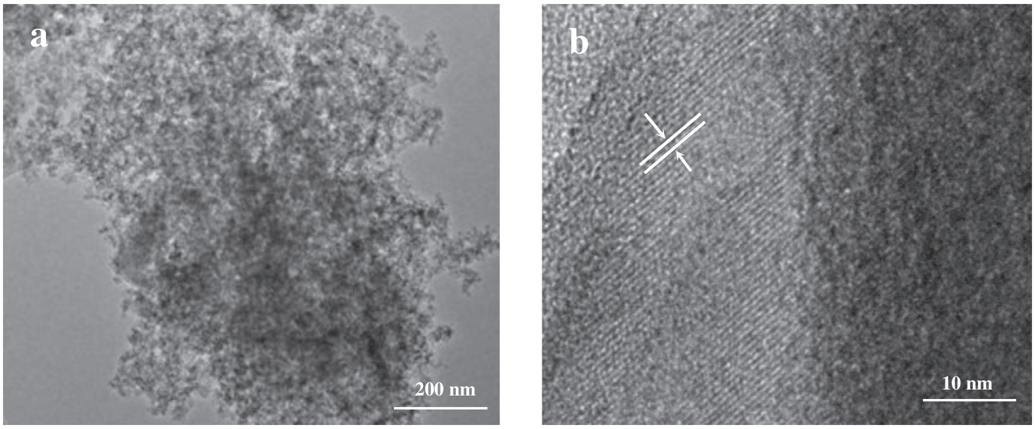

Fig. 3. TEM analysis of the selected 20 wt.% $H_4SiW_{12}O_{40}$-SiO_2: (a) at 200 nm; (b) at 10 nm.

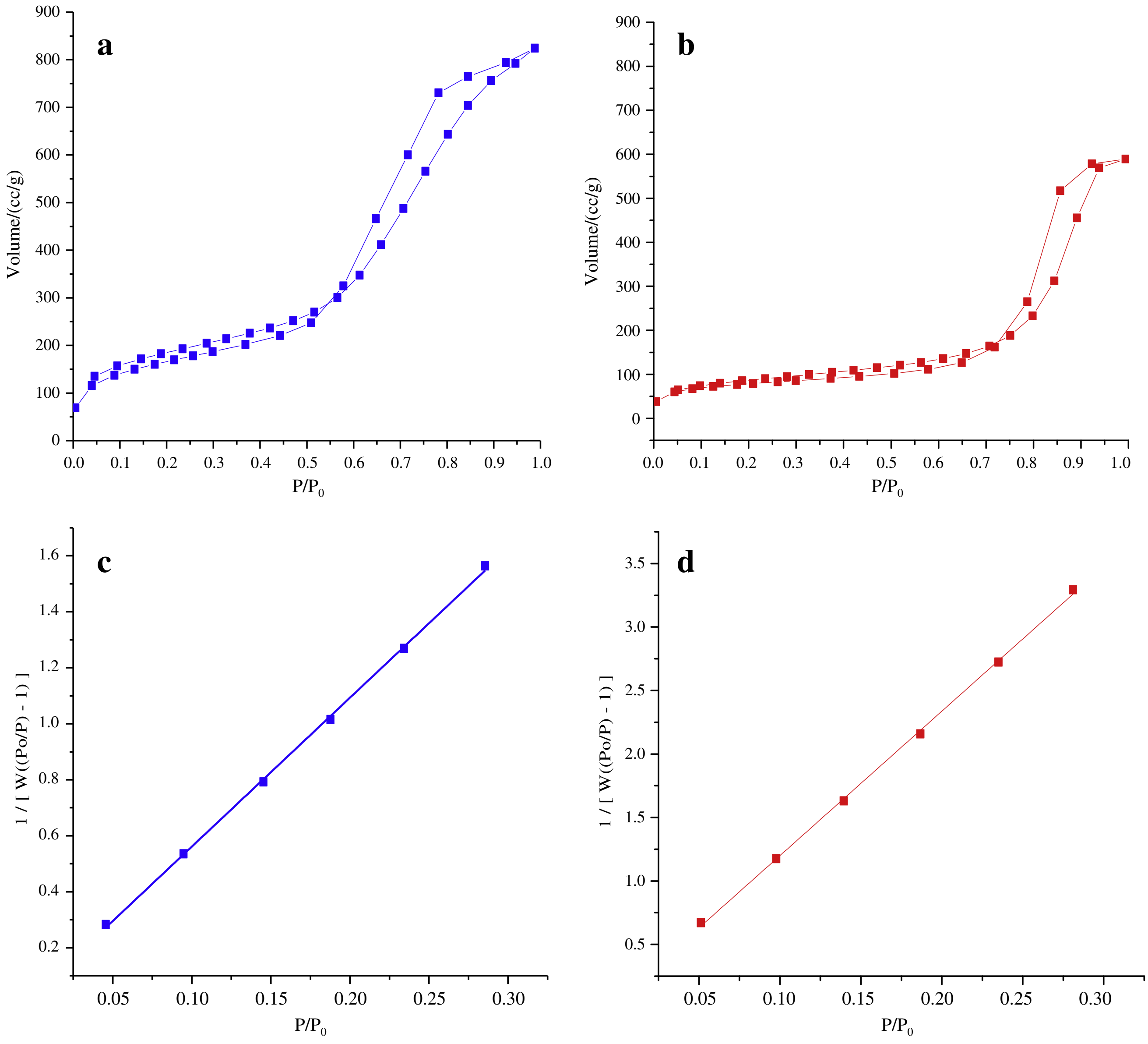

Fig. 4. Surface area and pore size analysis of mesoporous SiO_2 and 20 wt.% $H_4SiW_{12}O_{40}$-SiO_2: (a) N_2 adsorption and desorption curves of mesoporous SiO_2; (b) N_2 adsorption and desorption curves of 20 wt.% $H_4SiW_{12}O_{40}$-SiO_2; (c) BET plot of mesoporous SiO_2; (d) BET plot of 20 wt.% $H_4SiW_{12}O_{40}$-SiO_2.

magnification TEM image (Fig. 3b) showed that the interplanar spacing of the $H_4SiW_{12}O_{40}$ nanoparticles was ~0.360 nm, which is in good agreement with the *d* value of the (222) planes of the body centered cubic $H_4SiW_{12}O_{40}$.

The introduction of $H_4SiW_{12}O_{40}$ into the silica network may influence the porous structure of the resultant samples [23,28]. Therefore, further N_2-BET analysis was performed. The N_2-isotherm and BET plots of two selected samples (mesoporous SiO_2 and 20 wt.% $H_4SiW_{12}O_{40}$-SiO_2) are depicted in Fig. 4. A typical IV curve of mesoporous materials was observed in the N_2-sorption isotherm. For the mesoporous SiO_2 (Fig. 4a), the steps on the adsorption isotherms were relatively wide, which exhibited capillary condensation at a relative pressure of ~0.58. In the case of 20 wt.% $H_4SiW_{12}O_{40}$-SiO_2 (Fig. 4b), the steps on the adsorption isotherms were relatively narrow and revealed the capillary condensation at a relative pressure of ~0.75. BET plots (Fig. 4c and d) were used to evaluate the surface area and pore size of the resulting samples. In both cases the a_s plots revealed that the R-square was over 0.999, which confirmed that the fitting of linear and a_s plots were highly reliable. The surface areas and pore sizes of the resulting samples are presented in Table S1. With the exception of 40 wt.% $H_4SiW_{12}O_{40}$-SiO_2 (Table S1, No.

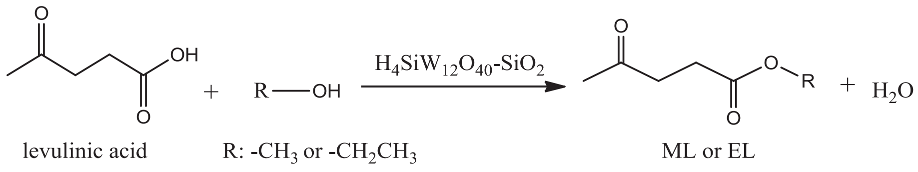

Scheme 1. Synthesis of methyl levulinate (ML) and ethyl levulinate (EL) using the mesoporous $H_4SiW_{12}O_{40}$-SiO_2 catalysts.

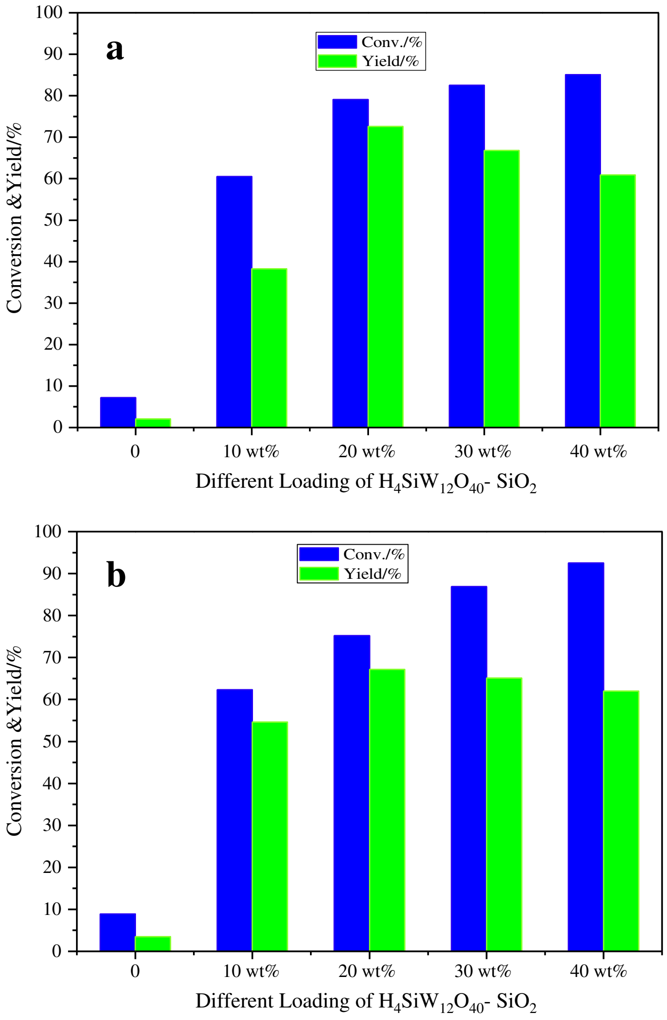

Fig. 5. Catalytic activities of $H_4SiW_{12}O_{40}$-SiO_2 in the synthesis of methyl levulinate (a) and ethyl levulinate (b) under the following conditions: m(levulinic acid) = 205 mg; V(cyclohexane) = 5 mL; m (catalyst) = 104 mg; and t = 6 h. To synthesize ML: V(methanol) = 2 mL and T = 65 °C. To produce EL: V(ethanol) = 2 mL and T = 75 °C.

5), the remaining four samples exhibited a high BET surface area in the range of 130–650 m^2/g. When the $H_4SiW_{12}O_{40}$ loading was increased, from 0 to 40 wt.% (No. 1 to No. 5), the surface areas became smaller and smaller. However, their pore sizes significantly increased after the introduction of $H_4SiW_{12}O_{40}$ up to 30 wt.% as it was expected that the confined $H_4SiW_{12}O_{40}$ nanoparticles would swell the mesoporous SiO_2 channel.

3.2. Catalytic performance

The mesoporous $H_4SiW_{12}O_{40}$-SiO_2 catalysts were evaluated in the synthesis of ML and EL (Scheme 1):

The catalytic results are depicted in Fig. 5. In general, all of the resultant catalysts exhibited good performance in both reactions. The best activity was achieved on the 20 wt.% $H_4SiW_{12}O_{40}$-SiO_2 catalyst, where a 73% yield of ML was achieved at the 79% conversion of levulinic acid. In contrast, in a comparative reaction that utilized only the mesoporous SiO_2, ~2% ML was yielded at 7% conversion after 6 h, showing that $H_4SiW_{12}O_{40}$ was the active acidic center. In addition, when the $H_4SiW_{12}O_{40}$ loading was increased to 30 wt.%, 67% yield of ML was achieved at a conversion of 83%, which was slightly lower than the yield in the case of 20 wt.% $H_4SiW_{12}O_{40}$-SiO_2 catalyst. This demonstrated that the increased amount of $H_4SiW_{12}O_{40}$ would promote the reaction as indicated by the conversion of levulinic acid. However, on the other hand, it would simultaneously enhance the side reactions, for instance the etherification of methanol; thus the selectivity of ML would be reduced. With 40 wt.% $H_4SiW_{12}O_{40}$-SiO_2 as the catalyst, an only 61% yield was obtained. This is likely due to the significant decrease of the surface area (Table S1). For the catalytic synthesis of EL, the best catalytic performance was also observed with the 20 wt.% $H_4SiW_{12}O_{40}$-SiO_2 catalyst (Fig. 5b): a 67% yield of EL was achieved at 75% conversion of levulinic acid. The same trend for the production of ML and EL was observed in terms of the yield: 20 wt.% $H_4SiW_{12}O_{40}$-$SiO_2 >$ 40 wt.% $H_4SiW_{12}O_{40}$-$SiO_2 >$ 10 wt.% $H_4SiW_{12}O_{40}$-$SiO_2 >$ meso-SiO_2.

In order to test recycling properties, the spent catalyst (20 wt.% $H_4SiW_{12}O_{40}$-SiO_2) was separated through centrifugation following the reaction, dried at overnight at 120 °C, and then employed again for the catalytic tests. As shown in Table S2, a slight decrease of the performance (Run 2) was observed in both cases compared to the fresh catalyst (Run 1). During the second run, in the case of ML synthesis, a 60.2% yield was achieved at 74% conversion. For the EL synthesis, a 56% yield was obtained at 73% conversion. This decrease was likely due to the leaching of $H_4SiW_{12}O_{40}$ that was deposited on the surface of the mesoporous SiO_2. Our ICP analysis showed that ~1.0% of the $H_4SiW_{12}O_{40}$ was leached during Run 1. In the consecutive third and fourth runs, stable activity was achieved (Runs 3 and 4). No further leaching of tungsten was detected by ICP analysis, confirming that the resultant catalysts maintained stability.

4. Conclusion

Mesoporous $H_4SiW_{12}O_{40}$-SiO_2 catalysts with tunable compositions were successfully fabricated through a one-step method in the presence of a Brij 30 surfactant. The resultant catalysts were efficient for the synthesis of methyl levulinate and ethyl levulinate. The best performance of methyl levulinate (73% yield achieved at a 79% conversion) and ethyl levulinate (67% yield at a 75% conversion) was obtained using the 20 wt.% $H_4SiW_{12}O_{40}$-SiO_2 catalyst. The recyclability tests demonstrated that the resultant catalysts maintained stable catalytic activities, which is promising for general applications in the production of biodiesel fuels.

Acknowledgments

This work was supported by a Discovery Grant from the Natural Sciences and Engineering Research Council of Canada (NSERC) and the Centre for Research and Innovation in the Bio-Economy (CRIBE). K. Yan. appreciates the Ontario Postdoctoral Fellowship. A. Chen acknowledges NSERC and the Canadian Foundation of Innovation (CFI) for the Canada Research Chair Award in Material and Environmental Chemistry.

Appendix A. Supplementary data

Supplementary data to this article can be found online at http://dx.doi.org/10.1016/j.catcom.2013.01.010.

References

[1] G.W. Huber, S. Iborra, A. Corma, Chemical Reviews 106 (2006) 4044–4098.
[2] Y. Roman-Leshkov, C.J. Barrett, Z.Y. Liu, J.A. Dumesic, Nature 447 (2007) 982–986.
[3] E. Taarning, C.M. Osmundsen, X. Yang, B. Voss, S.I. Andersen, C.H. Christensen, Energy & Environmental Science 4 (2011) 793–804.
[4] D.J. Braden, C.A. Henao, J. Heltzel, C.T. Maravelias, J.A. Dumesic, Green Chemistry 13 (2011) 1755–1765.
[5] J.C. Serrano-Ruiz, J.A. Dumesic, Energy & Environmental Science 4 (2011) 83–99.
[6] E. Christensen, A. Williams, S. Paul, S. Burton, R.L. McCormick, Energy & Fuels 25 (2011) 5422–5428.
[7] E. Christensen, J. Yanowitz, M. Ratcliff, R.L. McCormick, Energy & Fuels 25 (2011) 4723–4733.
[8] D.M. Alonso, J.Q. Bond, J.A. Dumesic, Green Chemistry 12 (2012) 1493–1513.
[9] B.R. Moser, A. Williams, M.J. Haas, R.L. McCormick, Fuel Processing Technology 90 (2009) 112–1128.
[10] D.J. Hayes, Catalysis Today 145 (2009) 138–151.

[11] H. Joshi, B.R. Moser, J. Toler, W.F. Smith, T. Walker, Biomass and Bioenergy 35 (2011) 3262–3266.

[12] W.E. Erner, U.S. Patent 4,364,743, 1982.

[13] Y. Liu, E. Lotero, J.G. Goodwin Jr., Journal of Catalysis 242 (2006) 278–286.

[14] R. Ronnback, S. Salmi, A. Vuori, H. Haario, J. Lehtonen, A. Sundqvist, E. Tirronen, Chemical Engineering Science 52 (1997) 3369–3381.

[15] J. Lilja, D.Y. Murzin, T. Salmi, J. Aumo, P. Mäki-Arvela, M. Sundell, Journal of Molecular Catalysis A 31 (2002) 555–563.

[16] J. Sambeth, G. Romanelli, J.C. Autino, J. Thomas, G. Baronetti, Applied Catalysis A 378 (2010) 114–118.

[17] A. Engin, H. Haluk, K. Gurkan, Green Chemistry 5 (2003) 460–466.

[18] D.R. Fernandesa, A.S. Rochaa, E.F. Maia, C.J.A. Motab, V. Teixeira da Silva, Applied Catalysis A 425–426 (2012) 199–204.

[19] S. Saravanamurugan, A. Riisager, Catalysis Communications 17 (2012) 71–75.

[20] G. Pasquale, P. Vázquez, G. Romanelli, G. Baronetti, Catalysis Communications 18 (2012) 115–120.

[21] S.M. Kumbar, G.V. Shanbhag, F. Lefebvre, S.B. Halligudi, Journal of Molecular Catalysis A 256 (2006) 324–334.

[22] K. Okumura, S. Ito, M. Yonekawa, A. Nakashima, M. Niwa, Topics in Catalysis 52 (2009) 649–656.

[23] K.X. Li, J.L. Hu, W. Li, F.Y. Ma, L.L. Xu, Y.H. Guo, Journal of Materials Chemistry 19 (2009) 8628–8638.

[24] J. Dou, H.C. Zeng, Journal of the American Chemical Society 134 (2012) 16235–16246.

[25] A. Miyaji, T. Echizen, K. Nagata, Y. Yoshinaga, T. Okuhara, Journal of Molecular Catalysis A 201 (2003) 145–153.

[26] B. Karmakar, A. Sinhamahapatra, A.B. Panda, J. Banerji, B. Chowdhury, Applied Catalysis A 392 (2011) 111–117.

[27] R.H. Tian, O. Seitz, M. Li, W. Hu, Y.J. Chabal, J.M. Gao, Langmuir 26 (2010) 4563–4566.

[28] Y.M. Luo, Z.Y. Hou, R.T. Li, X.M. Zheng, Microporous and Mesoporous Materials 109 (2008) 585–590.